

Beam-Impedance Considerations for the EIC HSR Screen

S. Verdu-Andres

September 2023

Electron-Ion Collider
Brookhaven National Laboratory

U.S. Department of Energy
USDOE Office of Science (SC), Nuclear Physics (NP)

Notice: This technical note has been authored by employees of Brookhaven Science Associates, LLC under Contract No. DE-SC0012704 with the U.S. Department of Energy. The publisher by accepting the technical note for publication acknowledges that the United States Government retains a non-exclusive, paid-up, irrevocable, world-wide license to publish or reproduce the published form of this technical note, or allow others to do so, for United States Government purposes.

DISCLAIMER

This report was prepared as an account of work sponsored by an agency of the United States Government. Neither the United States Government nor any agency thereof, nor any of their employees, nor any of their contractors, subcontractors, or their employees, makes any warranty, express or implied, or assumes any legal liability or responsibility for the accuracy, completeness, or any third party's use or the results of such use of any information, apparatus, product, or process disclosed, or represents that its use would not infringe privately owned rights. Reference herein to any specific commercial product, process, or service by trade name, trademark, manufacturer, or otherwise, does not necessarily constitute or imply its endorsement, recommendation, or favoring by the United States Government or any agency thereof or its contractors or subcontractors. The views and opinions of authors expressed herein do not necessarily state or reflect those of the United States Government or any agency thereof.

Beam-Impedance Considerations for the EIC HSR Screen

Silvia Verdú-Andrés*

Brookhaven National Laboratory
Upton, NY 11973 (USA)

(EIC Project)

(Dated: September 27, 2023)

The hadron storage ring (HSR) of the Electron-Ion Collider (EIC) will use the superconducting magnets from the Relativistic Heavy Ion Collider (RHIC). However, the beam pipes of these magnets show too large resistive-wall impedance and secondary electron yield to the HSR beams. The planned solution is to install beam screens that feature a thin film of amorphous carbon with low SEY on top of a high RRR copper layer for reduced impedance. This note discusses beam-impedance considerations that impact the EIC HSR beam screen design.

I. INTRODUCTION

The hadron storage ring (HSR) of the Electron-Ion Collider (EIC) will use the superconducting magnets from the Relativistic Heavy Ion Collider (RHIC). However, the stainless steel beam pipes of these magnets show too large resistive-wall impedance to the HSR beams and too large secondary electron yield that would lead to electron cloud buildup. The planned solution is to install beam screens that feature a thin film of amorphous carbon with low SEY to suppress electron cloud buildup on top of a high RRR copper clad stainless steel wall for reduced impedance [1]. The latest screen profile has the racetrack cross section shown in Fig. 1. The racetrack profile is adopted for the screen to incorporate a cooling pipe and to enable the use of tooling that will assist in the insertion and installation of the screens into the beam pipes of the magnets while still providing a large horizontal aperture given that at some beam energies, the beam will circulate with large horizontal offsets.

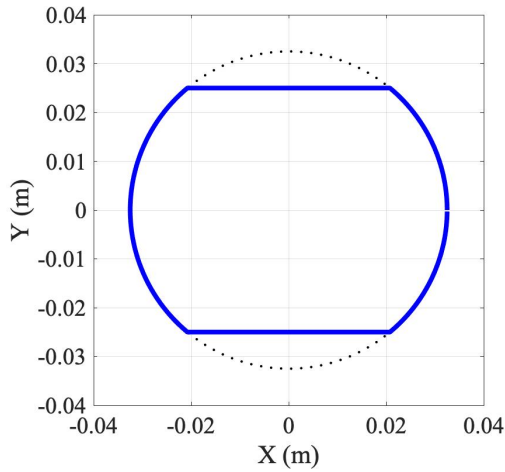


FIG. 1. Racetrack screen profile.

A. Resistive-wall heating in the round beam pipe of a circular accelerator by a uniformly-filled bunched beam

Assuming a uniformly-filled bunched beam with M bunches, the resistive-wall heating or power loss in a round beam pipe with RF surface resistance R_s is:

$$P_M = \frac{Q^2 M \mathcal{L}}{2\pi^2 b T_0} \int_0^{+\infty} d\omega R_s(\omega) h(\omega) \quad (1)$$

where T_0 is the revolution period of a single bunch traveling in a circular orbit of length \mathcal{L} ($T_0 = \mathcal{L}/(\beta c_0)$), the factor Q/T_0 is simply the average bunch current I_b , Q is the bunch charge, and b is the beam pipe radius. The R_s for the metallic walls of the beam pipe in the normal skin regime is:

$$R_s(\omega) = \sqrt{\frac{\omega \mu}{2\sigma_c}} = \frac{1}{\delta \sigma_c} \quad (2)$$

where ω is the angular frequency ($\omega = 2\pi f$) for a given eigenmode with resonant frequency f , μ is the electrical permeability, σ_c is the electrical conductivity, and δ is the skin depth ($\delta = \sqrt{2/\omega \mu \sigma_c}$). The power loss per unit of length P' for a beam with Gaussian bunches is:

$$P' = \Gamma \left(\frac{3}{4} \right) \frac{Q^2 M}{4\pi^2 b T_0} \sqrt{\frac{\mu}{2\sigma_c}} \left(\frac{1}{\sigma_t} \right)^{\frac{3}{2}} \quad (3)$$

where σ_t is rms bunch length.

B. Resistive-wall heating in the beam pipes of the RHIC superconducting magnets by EIC HSR beams. Rationale for the EIC HSR screens

Table I lists the EIC HSR proton beam parameters for several EIC beam scenarios. The proton beam for the highest center-of-mass energy E_{CM} scenario leads to the highest resistive-wall heating (per F_{QMS}). For the

* sverdu@bnl.gov

RHIC superconducting magnets with nominal, 69 mm-diameter, 4.55 K stainless steel beam pipe, this beam will deposit about 4 W/m in the beam pipe walls. Such large power is above the available dynamic heat budget of about 0.5 W/m [2]. Even for the RHIC magnets with larger apertures like the triplets (Q1, Q2, and Q3), with 113 mm-diameter beam pipe, the resistive-wall heating will exceed 2 W/m. This is due to the fact that for the EIC beam scenario driving resistive-wall heating, the number of bunches triples and the bunch shortens by an order of magnitude with respect to the corresponding RHIC beam, which only deposits about 0.05 W/m.

II. BEAM-IMPEDANCE OF EIC HSR SCREENS

This section discusses the impact of the wall surface layers and screen profile on the impedance presented by the HSR screens to the beam.

A. Amorphous carbon / Copper

The spectrum of the 60-mm rms long bunches for the highest energy (275 GeV) proton beams in the HSR goes up to about 2 GHz. In this frequency regime, the skin depth is much larger than the a-C film thicknesses under consideration for the EIC screens (hundreds of nm) and so the a-C film is considered a thin film as a significant portion of the beam-induced current will reach the subjacent layer of copper, as shown in Fig. 2. At the same time, the copper layer is sufficiently thick (tens of μm) for the current reaching the stainless steel sublayer to be negligible. In consequence, from now on, only the a-C and copper layers will be considered to evaluate the impact of the multilayers on the impedance of the screen.

The ImpedanceWake2D (IW2D) code computes longitudinal and transverse impedances for infinitely long multilayer structures [6]. The dependence of the beam screen impedance on the the a-C film thickness is evaluated from IW2D simulations of a round screen model with a thin a-C layer on an infinitely thick RRR 100 copper wall featuring the electromagnetic material properties listed in Table II. The RF surface resistance for a-C on Cu shown in Fig. 3 is computed from the IW2D longitudinal impedance, as for a round beam pipe:

$$\text{Re}\{Z_{\parallel}(\omega)\} = \frac{\mathcal{L}}{2\pi b} R_s(\omega) \quad (4)$$

The real component of the longitudinal impedance, associated to resistive-wall power losses, does not depend on the a-C thickness in the range of frequency of interest for a-C films as thick as few micrometers, as seen from Fig. 4. The dependence of the other impedance components on the a-C film thickness is shown in Figs. 4, 5 and 6. The imaginary component of the longitudinal

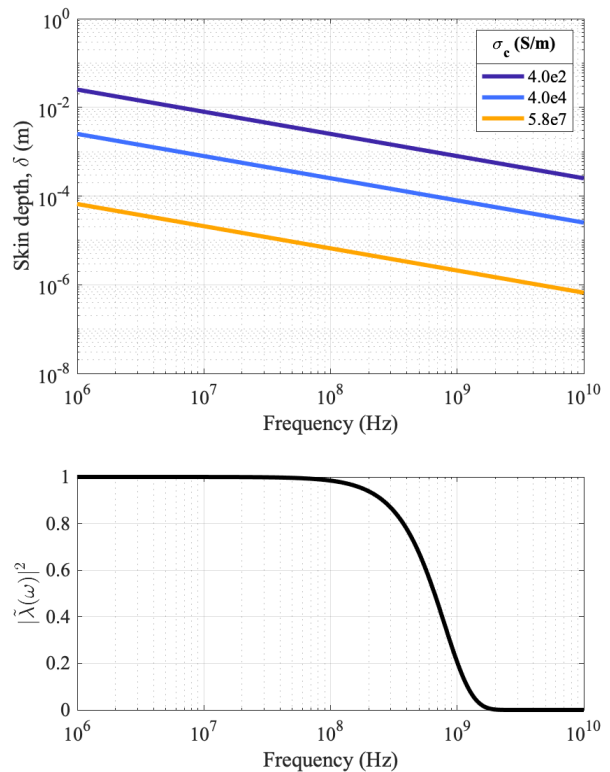


FIG. 2. Skin depth dependence on electrical conductivity for amorphous carbon (400 S/m [4] and 40000 S/m [5]) and room temperature copper (5.8e7 S/m) [top] and normalized spectral density of 60 mm rms-long Gaussian bunch [bottom]. Note that the skin depth will be even smaller for RRR copper at cryogenic temperatures.

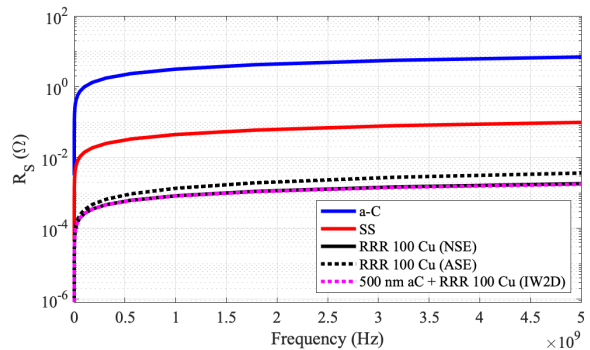


FIG. 3. RF surface resistance for several materials.

impedance is the most sensitive to the a-C film thickness. The plan is to deposit about 100-150 nm-thick layer of a-C on the screens, in which case the contribution from the a-C to the $\text{Im}\{Z_{\parallel}/n\}$ is negligible. In practice, coatings might not be as uniform as desired, and the film thickness could be slightly larger. Fig. 7 illustrates the imaginary component of the longitudinal impedance

TABLE I. Proton beam parameter values for different EIC beam scenarios [3].

Beam scenarios	275 GeV p + 18 GeV e (Highest E_{CM})	275 GeV p + 10 GeV e (Highest \mathcal{L})	100 GeV p + 10 GeV e	100 GeV p + 5 GeV e	41 GeV p + 5 GeV e
Energy (GeV)	275	275	100	100	41
No. bunches, M	290	1160	1160	1160	1160
Bunch spacing (ns)	40.59	10.15	10.15	10.15	10.15
Bunch charge, Q (10^{10})	19.1	6.9	6.9	4.7	2.6
RMS bunch length, σ_s (cm)	6	6	7	7	7.5
$F_{QMS} = Q^2 M / \sigma_t^{3/2}$ (a.u)	1	1/2.0	1/2.6	1/5.7	1/20

TABLE II. Material properties.

	Cu	a-C [4]
DC electrical resistivity, ρ_{dc} ($\Omega \cdot m$)	1/5.8e7	1/4e2
Dielectric constant, ϵ_r	1.0	5.4

normalized to the revolution harmonic, or effective longitudinal impedance $\text{Im}\{Z_{\parallel}/n\}$, for different copper RRR values and a-C thicknesses. The RRR value of copper is the dominant contributor to $\text{Im}\{Z_{\parallel}/n\}$ for a-C films thinner than 0.5 μm . Even for a 50 μm -thick a-C film, the imaginary component of the longitudinal impedance normalized to the revolution harmonic, $\text{Im}\{Z_{\parallel}/n\}$, is 0.6 Ω at 0.5 GHz, where $n = \omega/\omega_0$ and $\omega_0 = 2\pi f_{\text{rev}}$. This is smaller than the values for the two present RHIC rings, (1.5 ± 0.2) Ω and (5.4 ± 1.0) Ω , respectively, for the blue and yellow RHIC rings [7].

A few nm are sufficient to ensure low SEY [8]; however, to ensure sufficient coverage given expected thickness variations of the produced film, a target thickness of hundreds of nm should be adopted. This thickness is still sufficiently small to have a negligible impact on the impedance.

B. Anomalous skin effect in copper

Good conductors like copper experience the so-called anomalous skin effect at low temperatures and high frequencies, when the mean free path becomes comparable or greater than the classically calculated skin depth. In the anomalous skin regime, when $\alpha \rightarrow \infty$, the RF surface resistance can be calculated from an interpolation of the diffusion model [9]:

$$R_S = R_{\infty} (1 + 1.157\alpha^{-0.276}) \quad (5)$$

$$\alpha = \frac{3}{4}\omega\mu_0(\rho\lambda)^2\rho^{-3} \quad (6)$$

$$R_{\infty} = \left(\frac{\sqrt{3}}{16\pi} \rho\lambda (\omega\mu_0)^2 \right)^{1/3} \quad (7)$$

where the material-constant product $\rho\lambda = 6.6 \times 10^{-16}$ $\Omega \text{ m}^2$ for copper. Fig. 8 shows the RF surface resistance for RRR 100 copper calculated using the classical skin depth expression (Eq. 2) and the interpolation formula for the diffusion model (Ref. [9]) to the numerically calculated for the specular and diffusion reflection models [10]. The interpolation is close enough to the numerically computed curve.

For RRR 50 copper, the mean free path λ is comparable to the skin depth δ at $f \sim 24$ MHz; for RRR 100, that occurs at ~ 3 MHz. At higher frequencies of the EIC HSR beam spectra shown in Fig. 2, the skin depth is smaller than the mean free path and the anomalous skin effect becomes relevant. Fig. 9 shows how the RF surface resistance varies in function of frequency from that calculated from the classic skin depth when the anomalous skin effect is taken into account and Fig. 10 shows the spectral resistive-wall heating for the highest Ecm 275 GeV proton beam in a 35 mm-radius copper pipe calculated with Eq. 1 for the RF surface impedance with classic skin depth and anomalous skin effect. For the 275 GeV proton beam, which features 60 mm-rms-long bunches, the anomalous skin effect increases the resistive-wall heating of copper by a factor $F_{\text{ASE}} = 1.50$ when $\text{RRR} = 100$. For the 100 GeV proton beam, with 70 mm-rms-long bunches, $F_{\text{ASE}} = 1.47$. Fig. 11 shows the corrective factor to account for how the anomalous skin effect changes the resistive-wall heating in function of the copper RRR value.

C. Magneto-resistance

The electrical resistance of metals changes in presence of an externally-applied magnetic field. Longitudinal magneto-resistance, when the applied magnetic field is along the direction of the electric field, is generally smaller than transverse magneto-resistance, when the magnetic field is perpendicular to the electric field. For

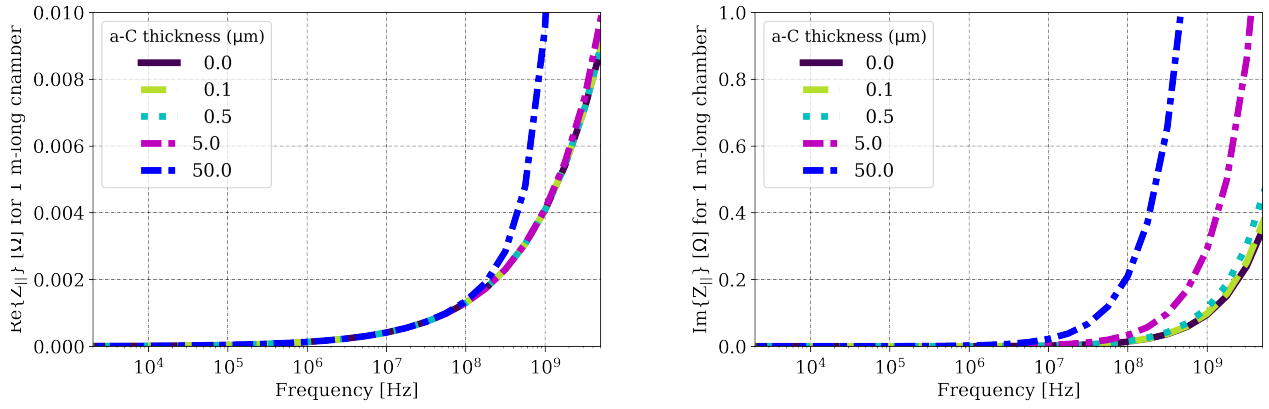


FIG. 4. Real and imaginary parts of the longitudinal impedance in function of the a-C film thickness.

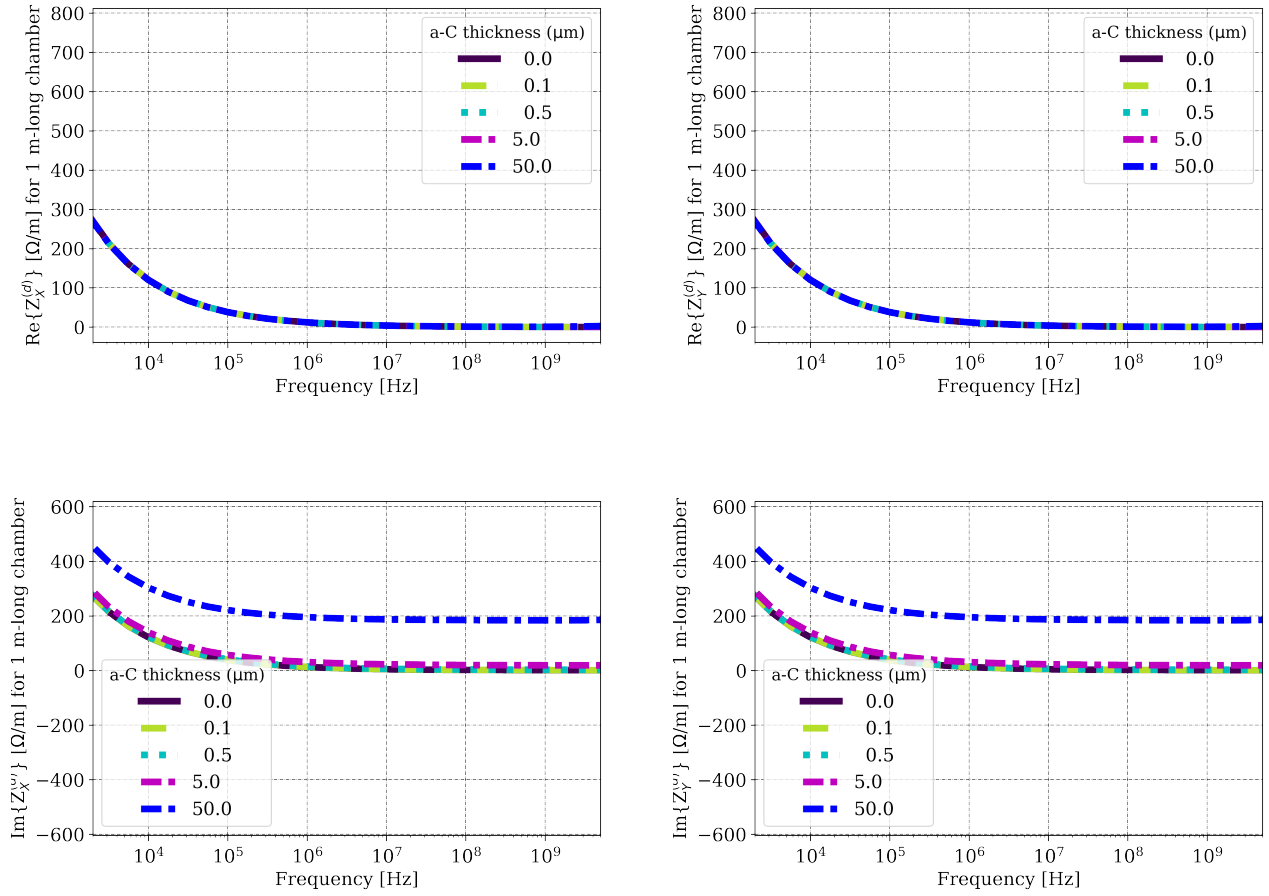


FIG. 5. Real (top) and imaginary (bottom) parts for the dipolar component of the transverse impedances in function of the a-C film thickness.

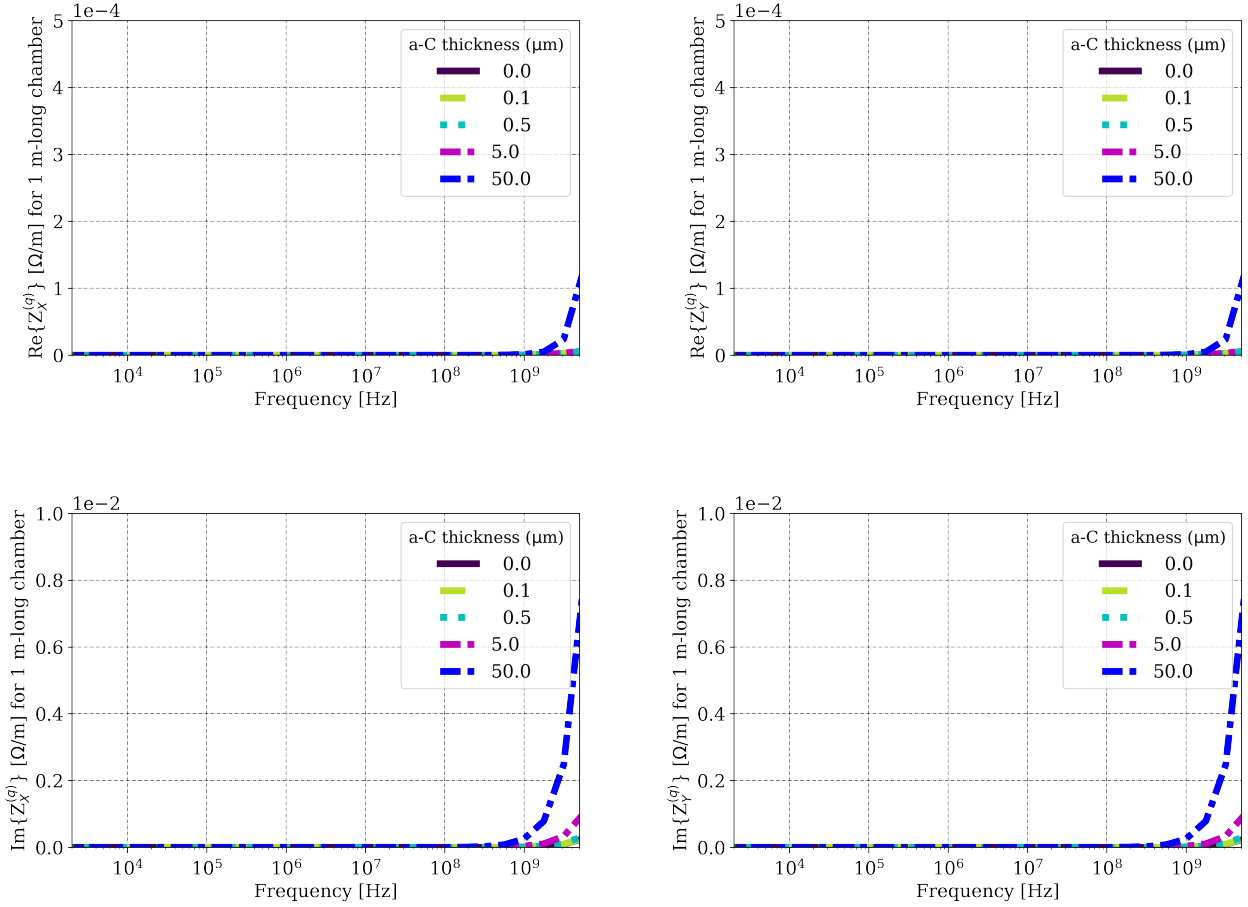


FIG. 6. Real (top) and imaginary (bottom) parts for the quadrupolar components of the transverse impedances in function of the a-C film thickness.

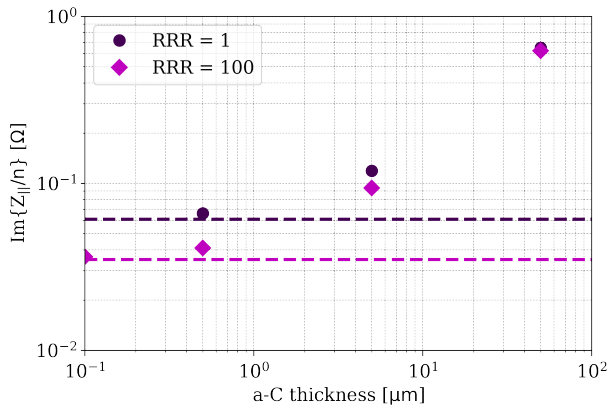


FIG. 7. Imaginary component of the effective longitudinal impedance in function of the a-C film thickness. The dotted lines represent the effective longitudinal impedance for a copper screen with no a-C film.

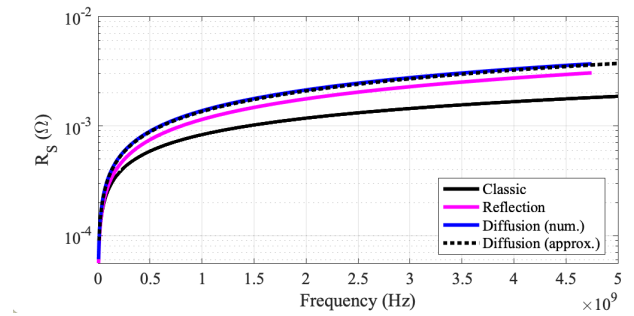


FIG. 8. RF surface resistance for $RRR = 100$ copper using the classical expression of skin depth and the interpolation formula for the diffusion model compared to the numerically computed for the specular and diffusion reflection models.

the beam screen, the magnetic field of the lattice magnets is perpendicular to the beam-induced currents and the DC electrical resistivity ρ of polycrystalline copper obeys Kolher's rule [11, 12] in Fig. 12, which can be fit-

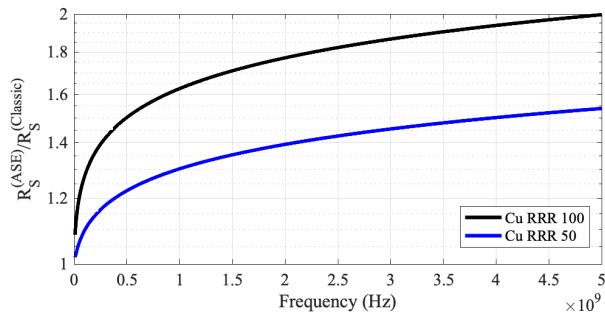


FIG. 9. Ratio between RF surface resistance with anomalous skin effect (ASE) and classic skin depth.

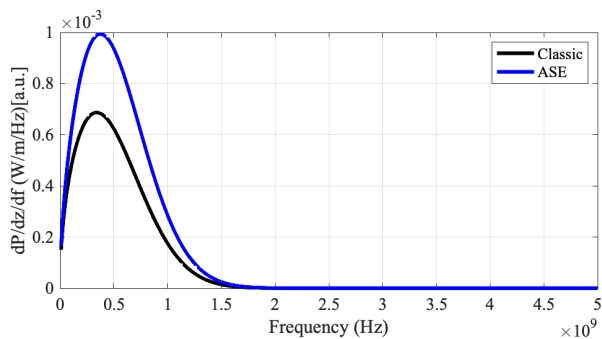


FIG. 10. Resistive-wall heating for 35 mm-radius pipe by the highest Ecm 275 GeV proton beam using the RF surface impedance for RRR 100 copper.

ted pretty well by the following expression [13]:

$$\frac{\Delta\rho}{\rho_0} = 10^{-2.69} (B[T] \times RRR)^{1.055} \quad (8)$$

where B is the magnetic field in tesla. The magneto-resistance increases the resistive-wall heating in the copper by a factor:

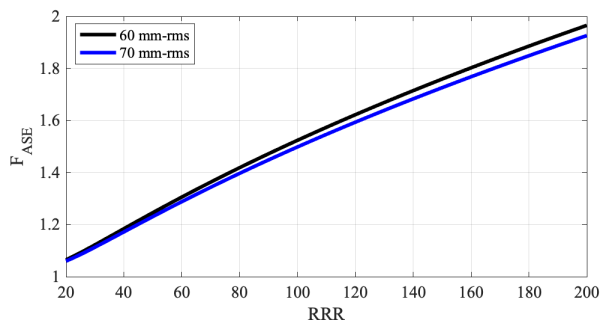


FIG. 11. Correction factor for power dissipation to incorporate anomalous skin effect for two different bunch lengths.

$$F_{MR} = \sqrt{1 + \frac{\Delta\rho}{\rho_0}} \quad (9)$$

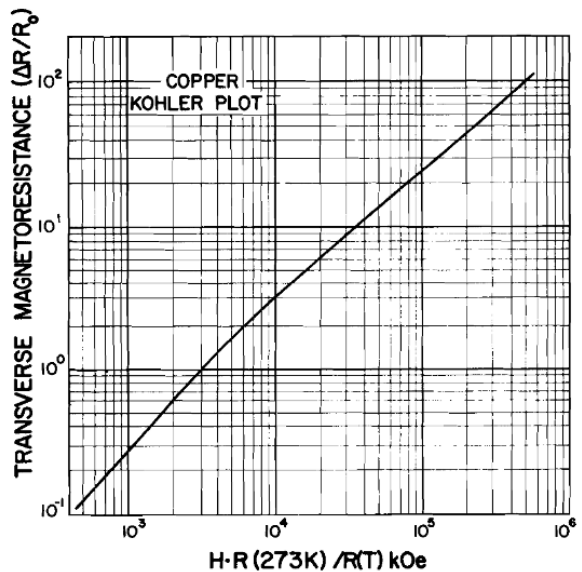


Fig. 2. Kohler plot for polycrystalline copper wires.

FIG. 12. Kohler's plot for transverse magneto-resistance of polycrystalline copper.

Figure 13 shows the dependence of F_{MR} on $B(T)$ for different values of RRR. The magneto-resistance contribution to the resistive-wall heating of the EIC HSR screen is computed using the magnetic field value at the cold bore location, not at the screen's perimeter. The magneto-resistance contribution for the on-axis 275 GeV proton beam optics is summarized in Table III. The rigidity of the 100 GeV proton beam is 2.73 times smaller. Assuming a direct scaling of the magnet strengths with the beam rigidity, the magneto-resistance contribution for the 100 GeV proton beam optics is that shown in Table IV. For regions with no magnetic fields, $F_{MR} = 1$.

The bunched beam induces RF currents on the walls of the beam screen (see Fig. 2). However, our calculations ignore that, for polycrystalline copper at 4.4 K, the RF magneto-resistance at GHz-level is one order of magnitude smaller than the DC magneto-resistance [15], that is, the magneto-resistance contribution is overestimated. Under the blunt assumption that ASE and magneto-resistance do not interplay, the reduction of resistive-wall heating by using high RRR copper is limited to a factor 4.5 to 6.25 by the anomalous skin effect and the magneto-resistance, in contrast to the factor 10 that one would naïvely expect for RRR 10 by the relationship $P' \propto 1/\sqrt{RRR}$. Fig. 14 shows that there would be a sweet point that enables the lowest resistive-wall heating for RRR ϵ [40, 100] in presence of high magnetic fields.

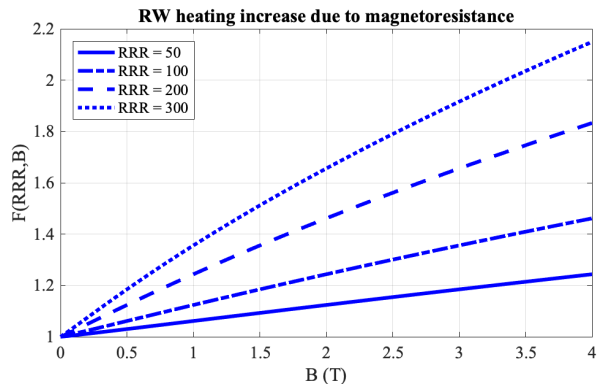


FIG. 13. F_{MR} for different RRR values as a function of $B(T)$ computed using the fit of Kohler's plot in Eq. 8.

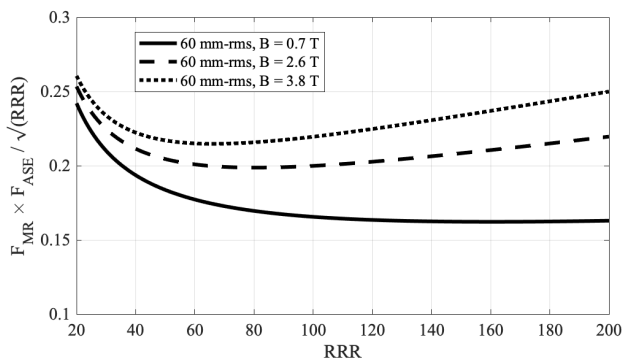


FIG. 14. Dependence of RRR-dependent factors on RRR.

D. Circular vs Racetrack profile

The resistive-wall power loss for a circular profile screen was evaluated 1) from the analytical expressions presented in Section IA and 2) numerically with the wakefield solver of CST Particle Studio. For the on-axis beam, the resistive-wall power loss per unit of length provided by CST simulations deviates only 1% from the expected value given by the analytical expression, while for the off-axis beam, the difference is still a reasonable 4%. The results of both approaches are compared in Table V. The good agreement between the value provided by CST simulations and the analytical expression enables the use of CST simulations for geometries that do not have an analytical expression like the racetrack profile. Results for the racetrack profile are also shown in Table V, with the racetrack profile featuring a resistive-wall power loss that is about 20% larger than that of a circular profile with the same horizontal aperture. The larger resistive-wall power loss is due to the flat walls being closer to the beam. All the CST simulations in Table V were done using the following settings:

- Model: 0.5 m-long pipe with normal conducting walls plus PEC material that extends for several mesh cells. Thick conducting wall to ensure at least

2 mesh cells.

- Mesh: about 500k hexahedral cells. Table VI shows the impact of mesh cell size and number on the accuracy of the resistive-wall power loss calculation.
- Ports: at least 10 modes to be calculated and accounted for in the simulation.
- Background: PEC
- Wake length: 1000 m
- Wake integration method: direct or indirect draw the same results given that structure has a constant cross section.

E. Beam offset

To synchronize the collisions of the ultra-relativistic electron bunches with the hadron bunches, a radial shift or beam offset will be implemented for hadron beams of certain energies. In store, the beams will circulate on axis. In collision mode, the 275 GeV proton beams will circulate through the arcs with a maximum radial shift of about +20 mm, while the 100 GeV proton beams will do at about -20 mm. (EIC HSR Functional Specification F-HSR-SYS.5, see Ref. [16].)

For the circular pipe shown in Fig. 16 with radius b where the beam travels with a certain offset x , the total resistive-wall heating increase due to beam offset is given by the rational function [17, 18]:

$$F_{BO} = \frac{b^2 + x^2}{b^2 - x^2} \quad (10)$$

showing an angular dependency given by:

$$\frac{dF_{BO}(\theta)}{d\theta} = \left(\frac{b^2 - x^2}{b^2 + x^2 - 2bx \cos(\theta)} \right)^2 \quad (11)$$

where θ denotes the position of an arc with respect to the axis defined by the offset beam as depicted in Fig. 15. For $b = 32$ mm and $x = 21$ mm (*i.e.* $x/b \simeq 0.66$), the resistive-wall heating in a circular pipe increases by a factor $F_{BO} = 2.5$ due to the beam offset, as shown in Fig. 16, with the angular power distribution in the circular pipe for the offset beam being shown in Fig. 17. The value computed from CST simulations for an offset beam in a circular profile pipe is within 4% of the analytical expression. Results are compiled in Table V. Fig. 18 shows the azimuthal distribution of the resistive-wall heating generated by on-axis as well as off-axis beams evaluated from CST simulations for a racetrack screen divided in the 16 sections depicted in Fig. 19.

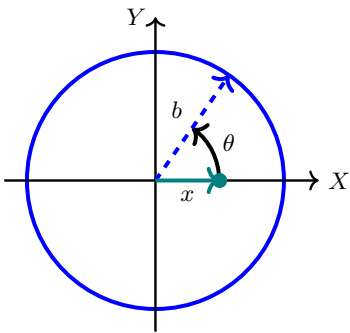


FIG. 15. Beam offset x (teal) in round beam pipe (blue) with radius b .

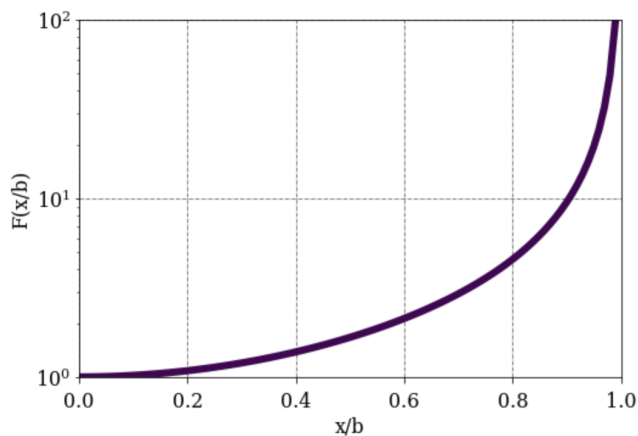


FIG. 16. Increase of resistive-wall heating with beam offset.

III. CONCLUSIONS

One of the two main functions of the EIC HSR screens is to reduce the impedance of the current RHIC beam pipe. The results of this study are useful to eval-

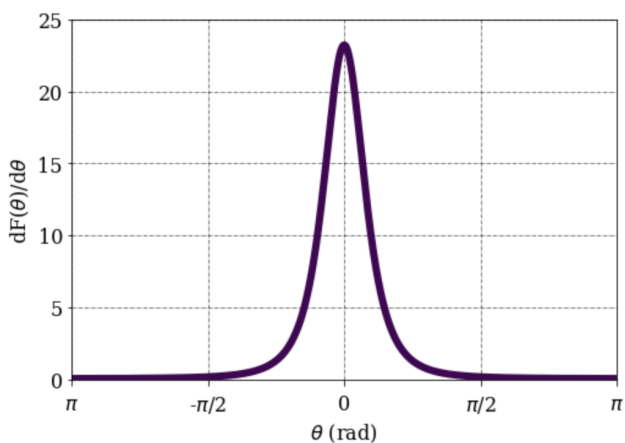


FIG. 17. Angular resistive-wall heating distribution in 32 mm-radius circular pipe due to 21 mm off-centered beam.

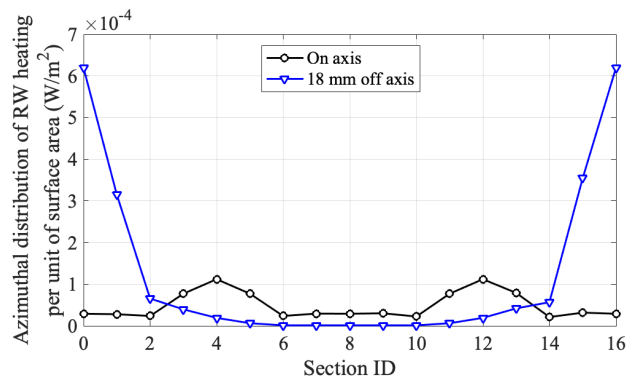


FIG. 18. Azimuthal resistive-wall heating distribution evaluated from CST simulations for a racetrack profile screen with $\sigma_c = 7690000$ S/m divided in 16 sections generated by on-axis and 18 mm off-axis single-bunch beams (1 nC bunch charge, 60 mm rms bunch length).

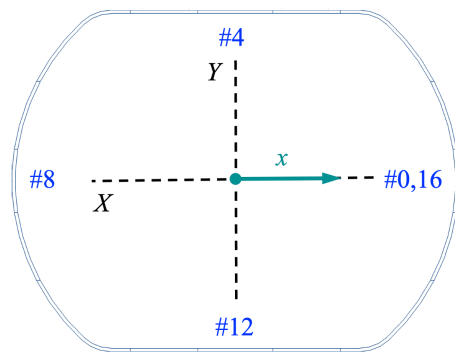


FIG. 19. Racetrack profile screen divided in 16 sections. Variable x designates the beam position.

uate the impact of some material properties on the beam-impedance, evaluate the contribution of the screen impedance to the heat load budget and define important screen specifications like the a-C film nominal thickness and thickness tolerance to ensure sufficient coverage, low SEY and no impact on impedance, and the necessary copper RRR value for low impedance. The resistive-wall heating for the HSR screen including welds and pumping slots is discussed in Ref. [19]. The geometric beam-impedance of the HSR screen with a preliminary pumping slots pattern is presented in Ref. [20].

ACKNOWLEDGMENTS

I am grateful to Mike Blaskiewicz, Boris Podobedov, Peter Thieberger (BNL), Benoit Salvant and Nicolas Mounet (CERN) for suggestions and useful discussions; and to Jingsong Wang (CST) for technical support to set up accurate resistive-wall power loss calculations in CST.

-
- [1] F. Willeke and et al., *Electron Ion Collider Conceptual Design Report*, Tech. Rep. (Brookhaven National Laboratory, 2021).
- [2] S. K. Nayak, S. Verdú-Andrés, M. Mapes, J. Tuozolo, and D. Weiss, Thermal analysis of RHIC arc dipole magnet cold mass with EIC beam screen, Tech. Rep. EIC-ADD-TN-028; BNL-222933-2022-TECH [10.2172/1863884](https://arxiv.org/abs/10.2172/1863884) (2022).
- [3] V. Ptitsyn, eRHIC parameter table v.6.
- [4] B. Salvant, Private communication, B. Salvant (CERN BE, May 12, 2021).
- [5] A. Passarelli, A. Andreone, M. De Stefano, C. Koral, M. R. Masullo, and V. Vaccaro, Broadband Frequency Electromagnetic Characterisation of Coating Materials, *JACoW IPAC2021, MOPAB346* (2021).
- [6] N. Mounet, Impedance Wake 2D (IW2D) Manual” (CERN BE, Geneva, 2014), <https://twiki.cern.ch/twiki/bin/view/ABPComputing/ImpedanceWake2D>.
- [7] M. Blaskiewicz, J. M. Brennan, and K. Mernick, Longitudinal Impedance of RHIC, in *6th International Particle Accelerator Conference* (2015) p. MOPMN020.
- [8] M. Angelucci, A. Novelli, L. Spallino, A. Liedl, R. Larciprete, and R. Cimino, Minimum thickness of carbon coating for multipacting suppression, *Phys. Rev. Res.* **2**, 032030 (2020).
- [9] W. Chou and F. Ruggiero, Anomalous Skin Effect and Resistive Wall Heating, LHC Project Note 2 (1995).
- [10] M. M. Blaskiewicz, Private communication on May, 2023: “surf3” Fortran code.
- [11] J. de Launay, R. Dolecek, and R. Webber, Magnetoresistance of copper, *Journal of Physics and Chemistry of Solids* **11**, 37 (1959).
- [12] F. R. Fickett, Magnetoresistivity of Copper and Aluminum at Cryogenic Temperatures, eConf **C720919**, 539 (1972).
- [13] E. Metral, Beam screen issues, in *Proc. of EuCARD-AccNet-EuroLumi Workshop: The High-Energy Large Hadron Collider* (2010).
- [14] S. Berg, Private communication, S. Berg: “275 GeV hadron ring lattice for beams on store (on-axis)” (BNL, Aug. 2022).
- [15] J. T. Rogers, S. De Panflis, A. C. Melissinos, B. E. Moskowitz, Y. K. Semertzidis, W. Wuensch, H. J. Halam, A. G. Prodell, W. B. Fowler, and F. A. Nezrick, Anomalous RF magnetoresistance in copper at 4-degrees K, UR-1043, ER-13065-521 (1988).
- [16] C. Cullen, *General and Functional Requirements for the Hadron Storage Ring System*, Tech. Rep. (Brookhaven National Laboratory).
- [17] R. T. Avery, A. Faltens, and E. C. Hartwig, Non-intercepting monitor of beam current and position, *IEEE Transactions on Nuclear Science* **18**, 920 (1971).
- [18] A. Piwinski, Wake fields and ohmic losses in round vacuum chambers, DESY-HERA-92-11 (1992), <https://lib-extopc.kek.jp/preprints/PDF/1992/9207/9207073.pdf>.
- [19] S. Verdú-Andrés and M. Sangroula, *Beam-induced heating in the EIC HSR screens*, Tech. Rep. (United States, 2023) (under preparation).
- [20] G. Wang, A. Blednykh, M. Sangroula, and S. Verdú-Andrés, *Updates on the Wake Potential Calculations for the Electron-ion Collider with ECHO3D*, Tech. Rep. (United States, 2023) (under preparation).

TABLE III. Magnetic strength k and maximum magnetic field B at 35 mm for on-axis 275 GeV proton beam optics [14] and magneto-resistance contribution to the DC electrical resistivity ρ of polycrystalline copper.

Magnet	k (T/m ⁿ)	Max. B[r = 35 mm] (T)	$\Delta\rho/\rho_0$ RRR = 50	F_{MR}	$\Delta\rho/\rho_0$ RRR = 100	F_{MR}
D	-3.782	3.8	0.5	1.23	1.1	1.44
QF / QD	-72.522 / +74.275	2.6	0.3	1.16	0.7	1.31
SF / SD	-368.877 / +577.077	0.7	0.1	1.04	0.2	1.09

TABLE IV. Magneto-resistance contribution to the DC electrical resistivity ρ of polycrystalline copper in 100 GeV proton beam optics.

Magnet	$\Delta\rho/\rho_0$ RRR = 50	F_{MR}	$\Delta\rho/\rho_0$ RRR = 100	F_{MR}
D	0.2	1.09	0.4	1.17
QF / QD	0.1	1.06	0.2	1.12
SF / SD	0.0	1.02	0.1	1.03

TABLE V. Resistive-wall power loss (in $\mu\text{W}/\text{m}$) for copper surface chambers ($\rho_{dc} = 1/5.8e7 \text{ Ohm} \cdot \text{m}$) with 32 mm radius circular profile and $a = 32 \text{ mm}$, $b = 24 \text{ mm}$ racetrack profile due to passage of a single 1 nC, 60 mm rms-long bunch. In parenthesis, relative error with respect to the analytical value.

	Circular		Racetrack
<i>On-axis</i>			
Analytical	2.79		–
CST	2.83	(1%)	3.40
<i>Off-axis, x = 21 mm</i>			
Analytical	7.00		–
CST	7.10	(4%)	6.86

TABLE VI. Mesh convergency study for computation of resistive-wall power loss with CST using 1000 m-long wake generated by 60 mm-long, 1 nC bunch travelling on-axis through a 0.5 m-long, 32 mm-radius copper pipe.

Mesh cells per wavelength	No. hexahedral mesh cells (k)	Simulation time (h)	P/L ($\mu\text{W}/\text{m}$)	Relative error w.r.t. analytical value (%)
40	148	8	3.01	8
60	468	25	2.92	5
75	892	34	2.83	1